An Updated Ultraviolet Catalog of *GALEX* Nearby Galaxies

Yu Bai, Hu Zou, JiFeng Liu, Song Wang

Key Laboratory of Optical Astronomy, National Astronomical Observatories, Chinese Academy of Sciences, 20A Datun Road, Chaoyang Distict, 100012 Beijing, China; ybai@nao.cas.cn, zouhu@nao.cas.cn, jfliu@nao.cas.cn, songw@nao.cas.cn

ABSTRACT

The ultraviolet catalog of nearby galaxies made by Gil de Paz et al. (2007) presents the integrated photometry and surface brightness profiles for 1034 nearby galaxies observed by *Galaxy Evolution Explorer* (*GALEX*). We provide an updated catalog of 4138 nearby galaxies based on the latest Genral Release (GR6/GR7) of *GALEX*. These galaxies are selected from HyperLeda with apparent diameter larger than $1'$. From the surface brightness profiles accurately measured with the deep NUV and FUV images, we have calculated asymptotic magnitudes, aperture (D25) magnitudes, colors, structural parameters (effective radii and concentration indices), luminosities, and effective surface brightness. Archival optical and infrared photometry from HyperLeda, 2MASS, and IRAS are also integrated into the catalog. Our parameter measurements and some analyses are consistent with those of Gil de Paz et al. (2007). The (FUV $-K$) color provides a good criterion to distinguish early and late-type galaxies, which can be improved further with the concentration indices. The IRX-β relation is reformulated with our UV-selected nearby galaxies.

Subject headings: atlases — galaxies: fundamental parameters — galaxies: photometry — ultraviolet: galaxies

1. INTRODUCTION

Nearby galaxies ($z \lesssim 0.1$) are characterized by large angular scale and high apparent brightness, which can be studied in more details and with higher accuracy than high-redshift galaxies. For nearby galaxies, the ultraviolet (UV) imaging provides unique information. Massive, young stars emit strong UV energy, which dominates the integrated UV light of star-forming galaxies. Thus, the UV flux is widely used as an excellent and accurate measurement of the current star formation rate (SFR; Wilkins et al. 2012; Kennicutt 1998; Lanz Lauranne

2013). In addition, the interstellar dust can absorb the UV light and then re-emit at far-infrared wavelength. The comparison between infrared and UV emission can effectively trace the dust attenuation in galaxies. Radiative transfer models suggest that the ratio of far-infrared to UV luminosity is a reliable estimator of the dust attenuation (Buat & Xu 1996; Witt & Gordon 2000; Panuzzo et al. 2003), depending weakly on the geometry of stars and dust, the extinction law, and the stellar population.

The UV galaxy samples in the local universe are important for understanding the evolution of galaxies with cosmic time (Bouwens et al. 2012; Reddy et al. 2012; Ellis et al. 2013; Martin et al. 2005). There have been considerable attempts to explore the SFR, morphology, dust attenuation, and their evolutions by constructing UV-selected local galaxies (Sullivan et al. 2004; Calzetti et al. 1994; Buat et al. 2002; Kuchinski et al. 2000; Marcum et al. 2001; Lauger et al. 2005).

Based on *GALEX* Public Release 2 and 3 (GR2/GR3), Gil de Paz et al. (2007) (hereafter *GALEX* Atlas) presented a UV catalog of 1034 nearby galaxies selected from the Third Reference Catalog of Bright Galaxies (RC3; de Vaucouleurs 1991). They selected those galaxies whose optical diameters of the $\mu_B = 25$ mag arcsec^{-2} isophote (D25) are larger than $1'$. The FUV and NUV images were mainly taken from *GALEX* Nearby Galaxies Survey (NGS). From the surface brightness profiles, they obtained asymptotic magnitudes, colors, and concentration indices. In combination with archival optical and infrared data, they analyzed the color-magnitude and color-color diagrams, relations between colors and morphologies, IRX$-\beta$ relation, dust attenuation, and structural properties for different types of galaxies.

In February 2013, *GALEX* GR7 data was available. It includes more than 45000 images, almost three times larger than GR2/GR3. With deeper observations (up to 250 kilo-second), it is now possible to create a relative complete UV sample of nearby galaxies. In this work, we provide an updated UV catalog of nearby galaxies with deepest FUV and NUV images from GR6/GR7, archival optical and infrared photometry, and make some similar analysis to Gil de Paz et al. (2007).

In Section 2, we present our sample selection of nearby galaxies. In Section 3, the method of measuring the surface brightness profile is described in detail. The catalog content including the UV parameters and other archival data are described in Section 4. The parameter comparison of our catalog with *GALEX* Altas is shown in Section 5. Section 6 presents some analyses and application examples of our catalog. The summary is in Section 7. All magnitudes presented in the paper are corrected for the Galactic extinction using the Galactic Reddening Map of Schlegel et al. (1998). We use the reddening law of Cardelli et al. (1989) to convert $E(B-V)$ to the UV extinction: $A_{FUV} = 7.9E(B-V)$ and

$A_{NUV} = 8.0E(B-V)$.

2. Sample Selection

The nearby galaxies in this paper are extracted from HyperLeda [1] (Paturel et al. 2003; Makarov et al. 2014). HyperLeda is a catalog of extragalactic sources, which gives accurate coordinates of objects (typical accuracy better than $2''$), morphological parameters (e.g. size, axis ratio, position angle, morphogical type, etc.), and astrophysical parameters (optical magnitudes and colors, surface brightness, distance, kinematic quantities, etc.). It includes 3.7 million galaxies, much more than RC3 as used by Gil de Paz et al. (2007). The catalog provides Doppler distances for 20314 galaxies and redshift-independent distances for 2013 galaxies. Figure 1a shows the distributions of major-axis diameters in both HyperLeda and RC3 catalogs, while Figure 1b presents the same distributions but with D25 $> 1'$. The majority of HyperLeda galaxies have diameters less than $1'$, and over 99% RC3 galaxies are included in HyperLeda. The HyperLeda galaxies with diameters above $1'$ are more than those of RC3 by a factor of 3.

We adopt the same criterion of optical diameters as Gil de Paz et al. (2007) used, that is, D25 is larger than $1'$. There are 22948 galaxies satisfying this constraint. We retrieve FUV and NUV images for these galaxies from *GALEX* GR6/GR7 to obtain their intensity maps. Three imaging surveys are involved: Medium Imaging Survey (MIS), Nearby Galaxy Survey (NGS), and Deep Imaging Survey (DIS). We require the galaxies ($1.5 \times$ D25) to be fully covered by the *GALEX* field of view (FoV; 1.2° in diameter). Those galaxies with low signal-to-noise ratio or contaminated by surrounding galaxies and bright stars are excluded. The optical diameter D25 of M31 is about 3.0°, far beyond the *GALEX* FoV. We obtain 26 tiles of M31 in FUV and NUV from NGS and DIS, which are stacked to form very deep mosaics by Montage[2]. The final sample contains 4138 galaxies, 2321 of which have both FUV and NUV observations. There are 14 and 1803 galaxies having only FUV and NUV observations, respectively.

We present their basic parameters given by HypeLeda in Table 1, including the positions, sizes, morphological types and distances. For galaxies whose distances are not available, we get their distances from NED (the NASA/IPAC Extragalactic Database). There are 4047 galaxies with either luminosity distances or redshift-dependent distances.

---

[1] `http://leda.univ-lyon1.fr,revisedin2013July1`

[2] `http://montage.ipac.caltech.edu/`

Figure 2 shows the normalized distributions of D25 diameter, morphological type, and distance in *GALEX* Atlas and our sample. By contrast, our sample gives more galaxies with smaller diameters, earlier types, and larger distances.

3. Surface Brightness Measurement

GALEX provides sky background subtracted images, but the background near the galactic center is overestimated, especially for galaxies with large apparent sizes. We introduce a new procedure to better estimate the sky background, which is quite similar to the method in Zou et al. (2011). SExtractor (Bertin & Arnouts 1996) is used to separate source pixels from background pixels. The source pixels, together with the region with the galactocentric distance $r < 2\times$D25, are masked. Then, the remaining pixels are fitted with a two dimensional polynomial function to generate the background map. Finally, the fitted map is subtracted from the intensity image.

Foreground stars contaminate the galaxy flux and need to be masked in the intensity map. We get the point sources (mostly stars) within the image from *GALEX* photometric catalogs. The mask aperture is determined by the growth curve, where the corresponding aperture magnitude is close to the total magnitude presented in the catalog. However, the catalogued point sources might include some star formation regions, whose UV color is much bluer than normal stars. Since the number of star formation regions is strongly dependent on the galaxy type, we separate our entire sample into two subsamples according to the morphological type: one with T ≥ -0.5 identified as spiral/irregular galaxies (types from Sa to Irr) and the other with T < -0.5 identified as elliptical/lenticular galaxies (types from E to $S0a$). For early-type galaxies, all point sources detected by *GALEX* are regarded as foreground stars and masked. For late-type galaxies, we only mask the point sources with (FUV $-$ NUV) > 1, and keep bluer point sources with (FUV $-$ NUV) < 1 as star forming regions. The nuclei of galaxies, also point-like, are not masked. For galaxies with single UV-band observations, we define foreground stars by visually inspecting both the UV image and the color image of the Digitized Sky Survey.

We then use the MATLAB package of astronomy and astrophysics for the measurement (Ofek 2014). The radial surface brightness profile is computed with a series of elliptical annuli, whose major radii range from $3''$ to at least 1.5 times the D25 radius. The brightness errors are estimated with the method in Gil de Paz & Madore (2005). Figure 3 shows some examples of the false color images and surface brightness profiles of galaxies in our sample. The radial (FUV $-$ NUV) color profile is also plotted.

4. The Catalog Content

4.1. Asymptotic and D25 Magnitudes

We adopt the technique introduced by Cairós et al. (2001) to calculate the asymptotic magnitudes. First, the accumulated flux and the gradient of the growth curve at each radius are computed. Then, an appropriate radial range away from the galaxy center is visually chosen, where an error-weighted linear fit to the relation of accumulated flux vs. the gradient of the growth curve is performed. Finally, the intercept of this linear fit is regarded as the asymptotic magnitude, and corresponding magnitude error is derived from the error of the linear fit.

We also calculate the aperture magnitudes inside the D25 ellipses. The errors are estimated from the random noise inside the apertures and the uncertainties of the sky background subtraction (see Gil de Paz & Madore 2005). All the errors do not include the uncertainty of NUV and FUV photometric zeropoints, which are about 0.15 and 0.09 mag, respectively.

4.2. Effective surface brightness and concentration indices

Based on the growth curve, we derive the radii containing 50%, 20%, 25%, 75%, 80% of the total luminosity ($r_{\rm eff}$,r_{20}, r_{25}, r_{75}, and r_{80}, resepectively). The effective surface brightness is calculated as $I = 0.5L_{\rm FUV}/\pi r_{\rm eff}^2$ and the concentration indices are calucated as C31=r_{75}/r_{25} and C42 = 5log(r_{80}/r_{20}) (de Vaucouleurs 1977; Kent 1985).

4.3. Archival optical and infrared data

Multi-wavelength data of nearby galaxies could improve our understanding of their physical nature. We add some corollary data from other optical and infrared surveys into our catalog. HyperLeda provides the total B magnitude (B_T) and the total I magnitude (I_T). A total of 4064 galaxies have B_T magnitudes and 3265 galaxies have I_T magnitudes. There are 640 and 813 galaxies in our sample with $(U-B)_T$ and $(B-V)_T$ colors, respectively. In near infrared (NIR), we compile JHK-band photometry from the 2MASS Large Galaxy Atlas (LGA) (Jarrett et al. 2003). If galaxies are unavailable in LGA, JHK photometry in 2MASS Extended Source Catalog (XSC) are used. A total of 3708 galaxies have JHK magnitudes. In mid and far infrared (MIR and FIR), the photometry in 12μm, 25μm, 60μm and 100μm are obtained from Infrared Astronomical Satellite (IRAS). We follow the priority given by

Gil de Paz et al. (2007) to compile the photometry (Rice et al. 1988; Moshir & et al. 1990 and the *IRAS* Point Source Catalog). The 60μm and 100μm are used to estimate the far infrared emission. There are 1570 galaxies with infrared fluxes in both 60μm and 100μm. The UV properties and archival optical and IR data are presented in presented in Table 2 and Table 3, respectively.

5. Comparison with *GALEX* Atlas

We show the photometric comparisons between *GALEX* Atlas and our sample in Figure 4. Figure 4a–d display the differences of asymptotic and aperture magnitudes between our catalog and *GALEX* Atlas. There are 94% and 93% galaxies in the FUV and NUV with the difference of asymptotic magnitudes within 0.5 mag. We check the galaxies with differences larger than 0.5 mag and find that these differences might be caused by the different sky-background estimation and elliptical parameters inherited from their parent catalogues. We fit a sky background map for each galaxy, while *GALEX* Atlas only use a single background value. For example, the average background of PGC 4085 (ESO 243-G041) given by *GALEX* Atlas is 5.59×10^{-4} counts s^{-1} in the NUV, while the average value of our computed background is 2.24×10^{-3} counts s^{-1}, which leads to the magnitude difference of 0.59. After checking the intensity image, our fitted background is more reasonable, since the flux of no-signal area around the galaxies is about 2×10^{-3} counts s^{-1}. There are many galaxies in *GALEX* Atlas and our sample with different axis ratios and D25 diameters. When galaxies become fainter, the difference of the axis ratios can reach a factor of 9, which leads to different growth curves and results in different magnitudes. For example, the axis ratio of PGC 4190 (NGC 0407) given by HyperLeda is 6.9, while *GALEX* Atlas gives 4.3. These differences lead to the different magnitudes between *GALEX* Atlas and our sample.

Figure 4e and f show the differences between the (FUV-NUV) colors of asymptotic and aperture magnitudes. The colors of our sample is consistent with those in the catalogues of *GALEX* Atlas with standard deviations of 0.19 and 0.13 for asymptotic and aperture colors, respectively.

The differences of the concentration indices for the two samples are displayed in Figure 4g and h. The concentration indices in both FUV and NUV of our samples are on average smaller than those in *GALEX* Atlas, probably due to the differences of the growth curves.

6. Analyses and Some Applications

6.1. UV Properties of the galaxies

Figure 5 shows the distributions of UV properties of the galaxies in our catalog. Figure 5a-g presents the histograms of asymptotic magnitudes, morphological type, luminosities, (FUV − NUV) colors, effective radii, and concentration indices. The median asymptotic magnitudes in FUV and NUV are 17.55 and 17.20 mag, respectively. In our sample, about 5% galaxies show asymptotic magnitudes larger than D25 magnitudes. For these galaxies, the diameters corresponding to asymptotic magnitudes are smaller than the D25 diameters due to the lack of diffuse emission. The residual flux after background subtraction within D25 ellipses leads to additional UV flux in the D25 magnitudes.

There are 1030 (25%) and 2899 (70%) early and late-type galaxies (Figure 5b), and 209 (5%) galaxies without morphological types given by HyperLeda. Figure 5c presents the luminosity distributions . The median FUV and NUV luminosities are 7.8 $\times$ 10^8 and 9.1 $\times$ 10^8 $L_\odot$ (3.0 $\times$ 10^{35} and 3.5 $\times$ 10^{35} W), respectively. Ten galaxies in our catalog are ultraviolet-luminous galaxies (UVLGs; Heckman et al. 2005) defined as the FUV luminosity larger than 2×10^{10} $L_\odot$ (7.6×10^{36} W), which are extremely rare in the local universe. Among the ten galaxies, PGC 2248, 36466, 59214 have been identified by *GALEX* Atlas. PGC 53898 and 71035 are Seyfert galaxies (Véron-Cetty & Véron 2006). PGC 4007 and 17625 are a luminous infrared galaxies (LIRG; Haan et al. 2011; Sanders et al. 2003). The other three galaxies, PGC 23064, 30400, and 51865, are star-forming spiral galaxies with very UV-luminous arms. PGC 70348 (NGC 7469) is defined as a UVLG in *GALEX* Atlas but not qualified in our sample. Our FUV luminosity of this galaxy is about 7.3×10^{36} W , close to the threshold.

Figure 5d presents the color distributions of asymptotic and D25 magnitudes. The majority of galaxies has color bluer than (FUV − NUV) = 1, which has been used to separate foreground stars. The red tail of the distributions is populated by early-type galaxies. The distributions of effective radii in kiloparsecs are shown in Figure 5e. The median effective radii for FUV and NUV are 4.3 and 5.0 kpc, respectively. The distributions and comparisons of concentration indices are presented in Figure 5f-i. The galaxies are on average slightly more concentrated in the NUV than in the FUV by differences of 0.03 in C31 and 0.10 in C42, which may be due to the different fractions of the bulge component in spiral galaxies in these two bands (Gil de Paz et al. 2007). Figure 5j shows the color as a function of the FUV magnitude. The late-type galaxies are brighter and located in a narrow color range, while the early-type galaxies are fainter and distributed with broader and redder color span.

6.2. Effective Surface Brightness

The plot of effective surface brightness versus the FUV luminosity is presented in Figure 6. This figure shows a trend of slight increasing effective surface brightness with increasing luminosity, indicating that galaxies with large effective radii turn to be more luminous (Hoopes et al. 2007). **The effective surface brightness distribution of our sample is more concentrated than Hoopes et al. (2007) sample, since the contours in Figure 6 enclose 96% of the galaxies in our sample but only 84% in their sample.**

The compact UVLGs are UVLGs defined with a surface brightness $I_{FUV} > 10^9\ L_\odot\ \mathrm{kpc}^{-2}$ (Hoopes et al. 2007). They have characteristics that are remarkably similar to the Lyman break galaxies (LBGs), such as SFRs, metallicities, morphologies, kinematics, and attenuations (Hoopes et al. 2007; Overzier et al. 2008; Basu-Zych et al. 2007). Only 12 galaxies in our sample have the surface brightness $I_{\mathrm{FUV}} > 10^9\ L_\odot\ \mathrm{kpc}^{-2}$. Two of them, PGC 59214 and PGC 71035, have both high luminosity and high surface brightness, which can be classified as compact UVLGs. PGC 59214 is a BL Lac object and PGC 71035 is a Seyfert 1.5 (Véron-Cetty & Véron 2006). Both of them have very compact nuclei in the FUV, and the optically thick accretion disks around super-mass black holes probably dominates their FUV luminosity (Malkan &Sargent 1982; Ward et al. 1987; Sanders et al. 1989).

6.3. (FUV $-K$) tracing galactic morphology

Compared to the optical colors (Weiner et al. 2005; Pozzetti et al. 2010; Talia et al. 2014), the combination of UV and IR should be more efficient in separating the early and late-type galaxies, given their different SFRs and dust attenuation (Gil de Paz et al. 2007). Since the UV emission is very sensitive to the presence of recent star formation activity and the K band emission is sensitive to the accumulated star formation (Muñoz-Mateos et al. 2007), the (FUV $-K$) color provides a robust discrimination between early and late-type galaxies as analyzed by Gil de Paz et al. (2007).

Figure 7a shows the relation between (FUV $-K$) color and galactic morphology. Here we convert the 2MASS K band Vega magnitudes to the AB system by adding 1.84 mag (Muñoz-Mateos et al. 2009; Cohen et al. 2003). We calculate the dividing (FUV $-K$) color to separate early and late-type galaxies by minimizing the number of galaxies that are misclassified by the dividing magnitude, which leads to (FUV $-K$) = 6.84. About 68% early-type galaxies and 86% late-type galaxies are correctly classified. The (FUV $-K$) is linearly correlated to the morphology of late-type galaxies. The best linear fit to the relation

(green line in Figures 7) is

$$(\mathrm{FUV} - K) = (5.8 \pm 0.1) - (0.25 \pm 0.02) \times \mathrm{T}. \quad (1)$$

Here T is the morphological type given by HyperLeda and the errors of the parameters are derived from the linear fitting.

The concentration indices have also been used as a classification tool (Abraham et al. 1996; Bershady et al. 2000). The (FUV$-K$) color together with concentration indices are expected to show better separation of different type galaxies, which is discussed in Gil de Paz et al. (2007). We present the FUV concentration index C42 as a function of the (FUV $-K$) color in Figure 7b. Early-type galaxies have larger C42 and redder (FUV $-K$). The best separation line in the plane of this figure is computed as

$$(\mathrm{FUV} - K) = 14.4 \pm 0.3 - (2.5 \pm 0.1) \times \mathrm{C42_{FUV}}. \quad (2)$$

With this, 76% and 94% of early and late-type galaxies are correctly classified.

6.4. IRX-β relation

The IR excess (IRX) is widely used as a good tracer of the dust attenuation in galaxies, and the slope of the UV continuum (β) is considered as a proxy to estimate the IRX when IR data are not available, which is known as IRX-β relation (Daddi et al. 2007; Reddy & Steidel 2009; Takeuchi et al. 2010). IRX is defined as $\log(f_{\mathrm{TIR}}/f_{\mathrm{FUV}})$, where f_{TIR} is the total infrared flux, and β can be estimated by (FUV $-$ NUV). Here, the IRX-β relation is not valid for early-type galaxies, since a substantial part of dust heating is due to photons emitted by old stars which do not emit primarily in UV and the dust attenuation would be overestimated by IRX (Buat et al. 2011).

Figure 8 shows the (FUV $-$ NUV) color against IRX for our late-type galaxies together with the local starburst relation derived from Meurer et al. (1999). Here we define $f_{\mathrm{FUV}} = \lambda f_\lambda$ and adopt the formula proposed by Sanders & Mirabel (1996) to derive the f_{TIR}, which is estimated using the 12, 25, 60 and 100 μm from IRAS data. We separate our galaxies into two groups according to their FUV luminosities. In Figure 8, we can see that most of our galaxies are located below the relation of Meurer et al. (1999). The galaxies with brighter FUV luminosities ($L_{\mathrm{FUV}} \geq 10^{35} W$) have a tigher relation than that of fainter galaxies. Both groups have steeper IRX$-\beta$ relations than that of Meurer et al. (1999). We linearly fit the relations of these two groups, which are formulated as

$$\mathrm{IRX} = (6.54 \pm 0.01) \times (\mathrm{FUV} - \mathrm{NUV}) - (2.10 \pm 0.01), L_{\mathrm{FUV}} \geq 10^{35}\mathrm{W}, \quad (3)$$

$$\mathrm{IRX} = (2.76 \pm 0.05) \times (\mathrm{FUV} - \mathrm{NUV}) - (0.84 \pm 0.07), L_{\mathrm{FUV}} < 10^{35}\mathrm{W}. \quad (4)$$

7. SUMMARY

In this paper, we provide an updated catalog of 4138 nearby galaxies based on the latest (GR6/GR7) of *GALEX*, which is more than 3 times the number of galaxies in the original *GALEX* Atlas. Our samples are selected from the extragalactic catalog of HyperLinda. The D25 diameter is set to be larger than $1'$. Compared with *GALEX* Atlas, we apply a more precise procedure to estimate the sky background in the *GALEX* images. Radial FUV and NUV surface brightness profiles are obtained. From these profiles we calculate asymptotic magnitudes, aperture (D25) magnitudes, UV colors, structural parameters (effective radii and concentration indices), luminosities, and effective surface brightness. We also augment our data set with archival optical and infrared photometry from HyperLeda, 2MASS and IRAS. With this updated catalog, we confirm that the (FUV $-K$) color provides a good criterion to distinguish early and late-type galaxies, which can be improved further with the concentration indices. The IRX-β relation is reformulated with our UV-selected nearby galaxies.

The GALEX images and catalogs of our nearby galaxies can be accessed via the website `http://batc.bao.ac.cn/$\sim$zouhu/doku.php?id=projects:galax:start`

The authors acknowledge support from the National Science Foundation of China under grants NSFC-11273028, NSFC-11333004 and NSFC-11203031, and support from the National Astronomical Observatories, Chinese Academy of Sciences under the Young Researcher Grant. We thank Mark Seibert and Scott Fleming for providing subfunctions to generate false color images. We acknowledge the usage of the HyperLeda database[3]. This research has made use of the NASA/IPAC Extragalactic Database (NED), which is operated by the Jet Propulsion Laboratory, California Institute of Technology, under contract with the National Aeronautics and Space Administration. Some of the data presented in this paper were obtained from the Mikulski Archive for Space Telescopes (MAST). This research has made use of the NASA/IPAC Infrared Science Archive, which is operated by the Jet Propulsion Laboratory, California Institute of Technology, under contract with the National Aeronautics and Space Administration. This research made use of Montage, funded by the National Aeronautics and Space Administration's Earth Science Technology Office, Computation Technologies Project, under Cooperative Agreement Number NCC5-626 between NASA and the California Institute of Technology. Montage is maintained by the NASA/IPAC Infrared Science Archive.

[3] `http://leda.univ-lyon1.fr`

REFERENCES

Abraham, R. G., Tanvir, N. R., Santiago, B. X., et al. 1996, MNRAS, 279, L47

Basu-Zych, A. R., Schiminovich, D., Johnson, B. D., et al. 2007, ApJS, 173, 457

Bertin, E., & Arnouts, S. 1996, A&AS, 117, 393

Bershady, M. A., Jangren, A., & Conselice, C. J. 2000, AJ, 119, 2645

Bouwens, R. J., Illingworth, G. D., Oesch, P. A., et al. 2012, ApJ, 754, 83

Buat, V., Boselli, A., Gavazzi, G., & Bonfanti, C. 2002, A&A, 383, 801

Buat, V., Giovannoli, E., Takeuchi, T.T., et al. 2011, A&A, 529, 22

Buat, V., & Xu, C. 1996, A&A, 306, 61

Cairós, L. M., Caon, N., Vílchez, J. M. et al. 2001, ApJS, 136, 393

Calzetti, D., Kinney, A. L., & Storchi-Bergmann, T. 1994, ApJ, 429, 582

Cardelli, J. A., Clayton, G. C., & Mathis, J. S. 1989, ApJ, 345, 245

Cohen M., Wheaton W. A., & Megeath S. T., 2003, AJ, 126, 1090

Daddi, E., Dickinson, M., Morrison, G., et al. 2007, ApJ, 670, 156

de Vaucouleurs, G., 1977, Evolution of galaxies and stellar populations, ed. Larson R. B. & Tynsley B. M. (New Haven: Yale Univ. Obs.), 43

de Vaucouleurs, G., de Vaucouleurs, A., Corwin, H. G. et al. 1991, Third Reference Catalogue of Bright Galaxies (Berlin: Springer) (RC3)

Ellis, R. S., McLure, R. J., Dunlop, J. S., et al. 2013, ApJ, 763, L7

Gil de Paz, A., & Madore, B. F., 2005, ApJS, 156, 345

Gil de Paz, A., Boissier, S., Madore, B. F. et al. 2007, ApJS, 173, 185

Haan, S., Surace, J. A., Armus, L., et al. 2011, AJ, 141, 100

Heckman, T. M., Hoopes, C. G., Seibert, M. et al. 2005, ApJ, 619, 35

Hoopes, C. G., Heckman, T. M., Salim, S., et al. 2007, ApJS, 173, 441

Jarrett, T. H., Chester, T., Cutri, R., Schneider, S. E., & Huchra, J. P. 2003, AJ, 125, 525

Kennicutt, R. C., 1998, ARA&A, 36, 189

Kent, S. M., 1985, ApJS, 59, 115

Kuchinski, L. E., Freedman, W. L., Madore, B. F., et al. 2000, ApJS, 131, 441

Lanz Lauranne, Zezas Andreas, Brassington Nicola et al. 2013, ApJ, 768, 90

Lauger, S., Burgarella, D., & Buat, V. 2005, A&A, 434, 77

Malkan, M. A., & Sargent, W. L. W. 1982, ApJ, 254, 22

Makarov D., Prugniel P., Terekhova N., Courtois H., & Vauglin I. 2014, A&A, 570, A13

Marcum, P. M., O'Connell, R. W., Fanelli, M. N., et al. 2001, ApJS, 132, 129

Martin, D. C., Fanson, J., Schiminovich, D., et al. 2005, ApJ, 619, L1

Moshir, M., & et al. 1990, IRAS Faint Source Catalogue, version 2.0 (1990), 0

Meurer, G. R., Heckman, T. M., & Calzetti, D. 1999, ApJ, 521, 64

Muñoz-Mateos, J. C., Gil de Paz, A., Boissier, S., et al. 2007, ApJ, 658, 1006

Muñoz-Mateos J. C., Gil de Paz A., Zamorano J., et al. 2009, ApJ, 399, 444

Ofek, E. O. 2014, Astrophysics Source Code Library, 1407.005

Overzier, R. A., Heckman, T. M., Kauffmann, G., et al. 2008, ApJ, 677, 37

Panuzzo, P., Bressan, A., Granato, G. L., Silva, L., & Danese, L. 2003, A&A, 409, 99

Paturel, G., Petit, C., Prugniel, P., Theureau, G., Rousseau, J., Brouty, M., Dubois, P., Cambrésy, L., 2003, A&A, 412, 45

Pozzetti, L., Bolzonella, M., Zucca, E. et al. 2010, A&A, 523, 13

Reddy, N. A., Pettini, M., Steidel, C. C., Shapley, A. E., Erb, D. K., Law, D. R. 2012, ApJ, 754, 25

Reddy, N. A., & Steidel, C. C. 2009, ApJ, 692, 778

Rice, W., Lonsdale, C. J., Soifer, B. T., et al. 1988, ApJS, 68, 91

Sanders, D. B., Phinney, E. S., Neugebauer, G., Soifer, B. T., & Matthews, K. 1989, ApJ, 347, 29

Sanders, D. B., & Mirabel, I. F. 1996, ARA&A, 34, 749

Sanders, D. B., Mazzarella, J. M., Kim, D.-C., Surace, J. A., & Soifer, B. T. 2003, AJ, 126, 1607

Schlegel, D. J., Finkbeiner, D. P., & Davis, M., 1998, ApJ, 500, 525

Sullivan, M., Treyer, M. A., Ellis, R. S., & Mobasher, B. 2004, MNRAS, 350, 21

Takeuchi, T. T., Buat, V., Heinis, S., et al. 2010, A&A, 514, 4

Talia, M., Cimatti, A., Mignoli, M. et al. 2014, A&A, 562, 113

Ward, M., Elvis, M., Fabbiano, G., et al. 1987, ApJ, 315, 74

Véron-Cetty, M.-P., & Véron, P. 2006, A&A, 455, 773

Weiner, B. J., Phillips, A. C., Faber, S. M., et al. 2005, ApJ, 620, 595

Wikins, S. M., Gonzalez-Perez, V., et al. 2012, MNRAS, 427, 1490

Witt, A. N., & Gordon, K. D. 2000, ApJ, 528, 799

Zou, H., Zhang, W., Yang, Y. B. et al., 2011, AJ, 142, 16

Table 1. Our *GALEX* Sample of 4138 Nearby Galaxies

PGC	R.A. (J2000.0)	Dec. (J2000.0)	2×A (arcmin)	2×B (arcmin)	P.A. (deg)	T	Distance (Mpc)
(1)	(2)	(3)	(4)	(5)	(6)	(7)	(8)
12	00 00 08.604	−06 22 26.00	1.4	0.3	168	1.3 ± 1.0	95
62	00 00 46.908	−77 34 47.93	1.0	0.2	9	4.4 ± 1.9	153
120	00 01 38.316	+23 29 00.92	1.9	1.1	160	5.3 ± 1.5	52
129	00 01 41.916	+23 29 44.95	1.4	0.5	135	4.8 ± 1.4	65
143	00 01 58.188	−15 27 39.24	10.5	3.5	5	9.9 ± 0.3	0.97
176	00 02 34.836	−03 42 38.92	1.1	0.7	180	4.0 ± 0.5	93
192	00 02 48.624	−03 36 21.82	1.1	0.3	25	5.0 ± 2.0	90
215	00 03 14.184	−65 22 11.68	1.1	0.5	167	4.4 ± 1.9	90
243	00 03 32.148	−10 44 40.81	1.1	1.0	...	−2.0 ± 0.6	129
250	00 03 34.992	+23 12 02.92	1.0	0.6	23	5.5 ± 0.8	107
...	...	...	...	...	...	...	...

Note. — The parameters are taken from HyperLeda. For galaxies whose distances are not available, their distances are selected from NED. Col.(1): PGC number. Col. (2)–(3): R.A. and Dec. (J2000.0) of the galaxy center. Right ascensions are in hours, minutes, and seconds, and declinations are in degrees, arcminutes, and arcseconds. Col. (4): Major-axis diameter of the D25 ellipse. Col. (5): Minor-axis diameter. Col. (6): Position angle (P.A.). Col. (7): Morphological type T and its error. Col. (8): Distance in Mpc.

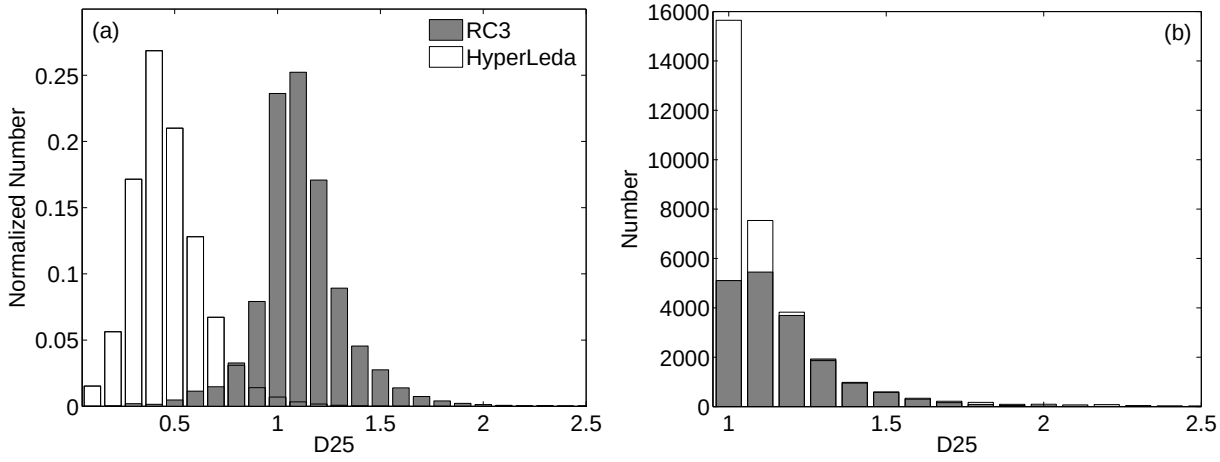

Fig. 1.— Comparison of D25 diameters in HyperLeada and RC3. (a) Normalized D25 distribution of major-axis diameters. (b) D25 distribution of major-axis diameters larger than 1′.

Table 2. UV Data in Our Catalog

PGC	Asymptotic Magnitudes		D25 Magnitudes		log L		Effective Radii		C31		C42	
	FUV (mag)	NUV (mag)	FUV (mag)	NUV (mag)	FUV (W)	NUV (W)	FUV (arcsec)	NUV (arcsec)	FUV	NUV	FUV	NUV
(1)	(2)	(3)	(4)	(5)	(6)	(7)	(8)	(9)	(10)	(11)	(12)	(13)
12	17.37 ± 0.01	16.93 ± 0.03	17.57 ± 0.01	17.18 ± 0.01	35.931	35.929	12.71	13.19	1.93	2.12	1.88	2.10
62	...	18.48 ± 0.04	...	18.70 ± 0.04	...	35.732	...	8.67	...	2.21	...	2.15
120	16.47 ± 0.04	15.90 ± 0.05	16.62 ± 0.01	16.01 ± 0.01	35.768	35.816	23.22	22.42	2.14	2.14	2.00	2.02
129	17.12 ± 0.03	16.50 ± 0.02	17.41 ± 0.02	16.70 ± 0.01	35.700	35.768	17.77	15.89	2.05	2.11	2.07	2.03
143	12.61 ± 0.04	12.41 ± 0.03	12.71 ± 0.00	12.52 ± 0.00	33.857	33.759	90.46	91.78	2.14	2.16	1.98	2.05
176	...	16.29 ± 0.07	...	16.50 ± 0.01	...	36.176	...	14.76	...	2.20	...	2.12
192	...	17.12 ± 0.02	...	17.21 ± 0.01	...	35.809	...	8.53	...	2.22	...	2.19
215	...	16.83 ± 0.04	...	17.04 ± 0.02	...	35.931	...	13.52	...	2.51	...	2.49
243	17.56 ± 0.05	16.96 ± 0.02	17.62 ± 0.01	17.05 ± 0.01	36.125	36.187	10.85	10.92	2.85	3.18	2.93	3.14
250	16.54 ± 0.08	15.97 ± 0.02	17.06 ± 0.01	16.41 ± 0.01	36.367	36.417	16.90	15.49	2.98	2.94	2.79	2.88

Note. — Col.(1): PGC number. Col. (2)–(3): Asymptotic magnitude and its error in the FUV and NUV. Cols. (4)–(5): The aperture magnitudes and their errors within the D25 ellipse in FUV and NUV, respectively. Col. (6)–(7): Logarithm of the FUV and NUV luminosity. Col. (8)–(9): Effective radii in the FUV and NUV. Col. (10)–(11): Concentration index C31 in the FUV and NUV. Col. (12)–(13): Concentration index C42 in the FUV and NUV.

Table 3. Achival Optical and Infrared Data in Our Catalog

PGC	Optical Magnitudes and Colors				2MASS Magnitudes			*IRAS* Fluxes			
	B	I	$(U-B)_T$	$(B-V)_T$	J	H	K	12μm	25μm	60μm	100μm
	(mag)	(mag)	(mag)	(mag)	(mag)	(mag)	(mag)	(Jy)	Jy	Jy	Jy
(1)	(2)	(3)	(4)	(5)	(6)	(7)	(8)	(9)	(10)	(11)	(12)
12	14.66 ± 0.38	...	...	...	12.10 ± 0.03	11.38 ± 0.04	11.11 ± 0.06	...	...	...	...
62	16.23 ± 0.21	14.47 ± 0.08	...	...	13.48 ± 0.08	12.73 ± 0.09	12.61 ± 0.14	...	...	...	...
120	13.01 ± 0.41	11.29 ± 0.22	...	...	10.33 ± 0.02	9.59 ± 0.02	9.33 ± 0.02	...	...	...	...
129	13.59 ± 0.30	12.43 ± 0.22	...	...	11.06 ± 0.02	10.16 ± 0.02	9.93 ± 0.03	< 0.38	< 0.67	5.47 ± 0.66	14.29 ± 1.86
143	10.89 ± 0.08	...	...	0.40	...	...	...	< 0.12	< 0.20	0.32 ± 0.08	1.04 ± 0.26
176	14.33 ± 0.29	12.77 ± 0.08	...	...	11.86 ± 0.03	11.24 ± 0.04	10.82 ± 0.05	< 0.25	< 0.33	1.21 ± 0.12	2.49 ± 0.27
192	15.07 ± 0.36	...	...	...	12.37 ± 0.03	11.69 ± 0.04	11.56 ± 0.07	...	...	...	...
215	15.49 ± 0.29	14.38 ± 0.08	...	...	14.09 ± 0.12	13.23 ± 0.15	12.99 ± 0.17	...	...	...	...
243	14.37 ± 0.36	12.50 ± 0.32	...	0.81	11.25 ± 0.03	10.63 ± 0.03	10.30 ± 0.04	0.11 ± 0.03	< 0.21	0.37 ± 0.05	1.58 ± 0.21
250	14.05 ± 0.54	12.25 ± 0.10	...	...	11.51 ± 0.04	10.83 ± 0.05	10.66 ± 0.06	< 0.25	< 0.25	0.74 ± 0.07	3.64 ± 0.66
...	...	...	...	...	...	...	...	...	...	...	...

Note. — Col.(1): PGC number. Col. (2): B-band total magnitude in Vega mag from HyperLeda. Col. (3): I-band total magnitudes in Vega mag from HyperLeda. Cols. (4)–(5): Total asymptotic $(U-B)$ and $(B-V)$ colors from HyperLeda. Cols. (6)–(8): 2MASS J, H, and K-band total magnitudes in Vega mag from (Jarrett et al. 2003) and the 2MASS Extended Source Catalog. Cols. (9)–(12): IRAS 12, 25, 60, and 100μm fluxes in Jy from (Rice et al. 1988; Moshir & et al. 1990) and the *IRAS* Point Source Catalog.

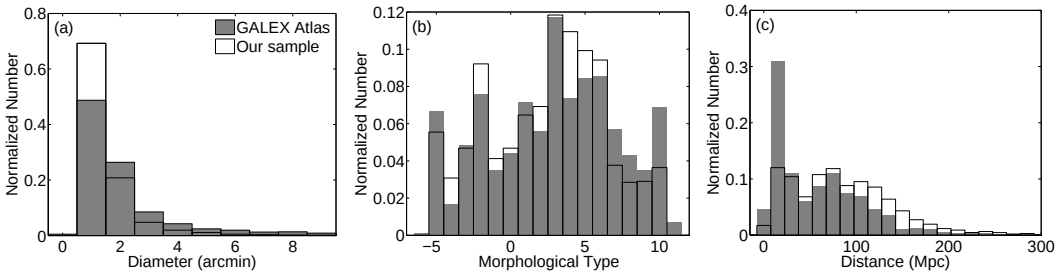

Fig. 2.— Comparison between the *GALEX* Atlas sample (grey-shade histogram) and our sample (solid line). (a) Major-axis diameters in arcmin. (b) Morphology type. (c) Distance in Mpc.

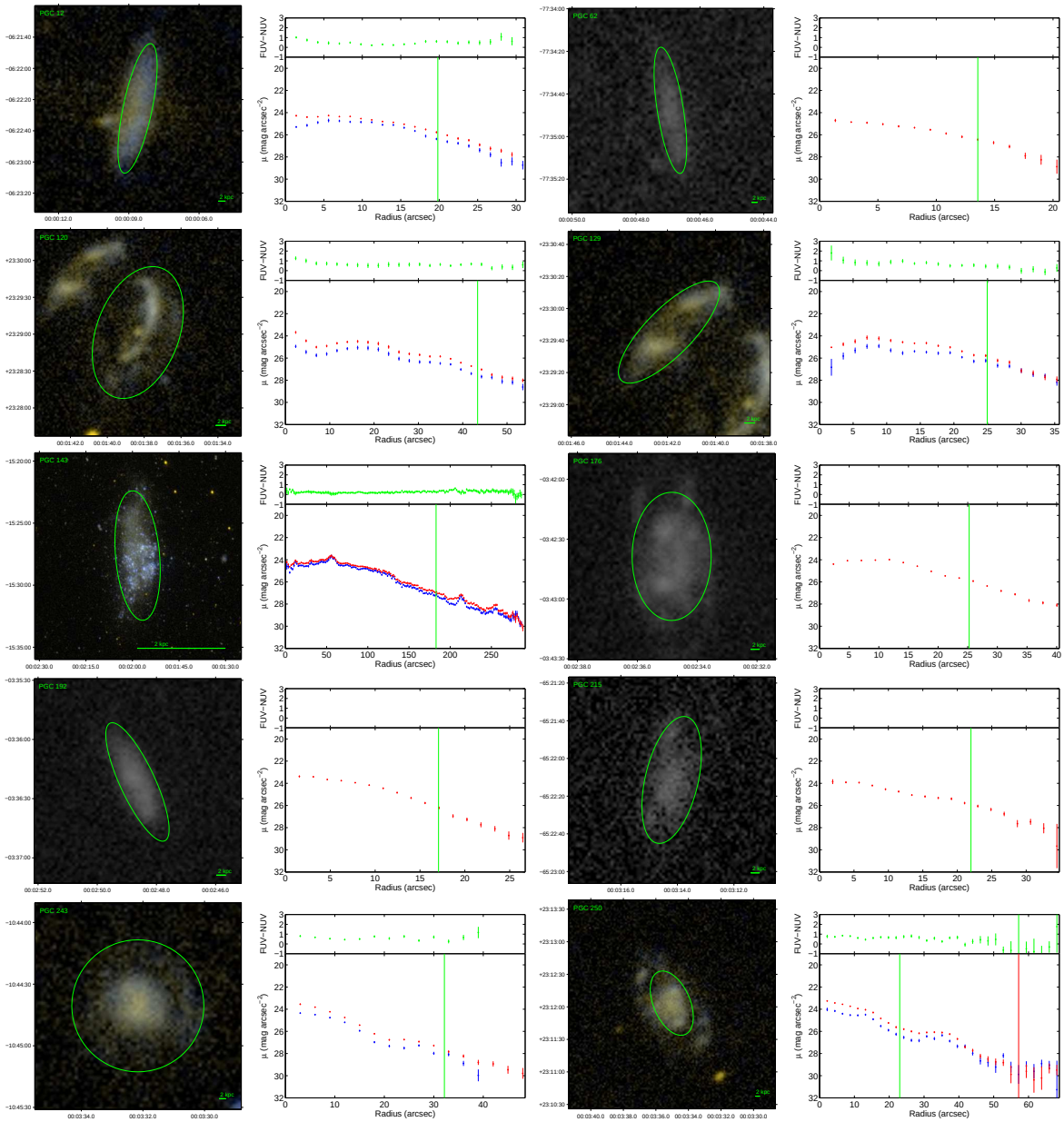

Fig. 3.— Left: False color images of our *GALEX* nearby galaxies. R.A. and Dec. are in J2000.0. The D25 ellipse is drawn in green. Right: radial surface brightness and color profiles. Red, blue, and green points present the NUV, FUV and (NUV − FUV) profiles, respectively. The green vertical line is the equivalent radius corresponding to D25.

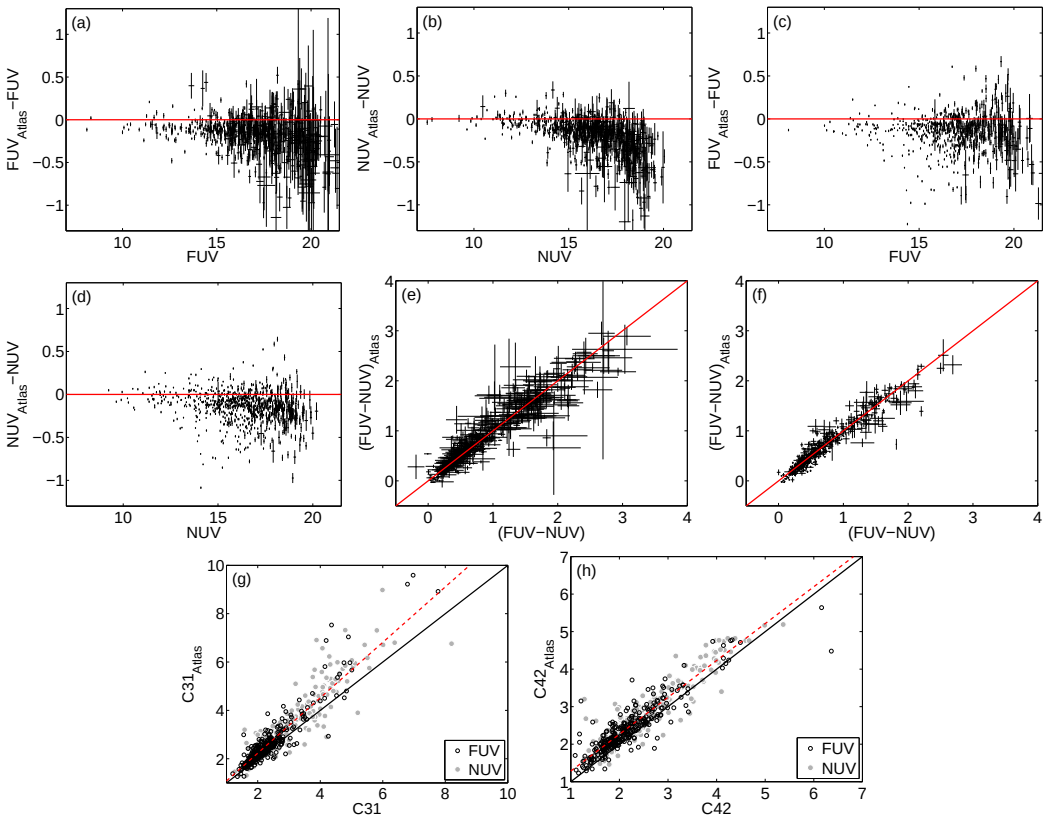

Fig. 4.— Photometric comparisons between the the *GALEX* Atlas and our catalog. *(a)–(b)* FUV and NUV asymptotic magnitudes difference between *GALEX* Atlas and our catalogs vs. asymptotic magnitudes in *GALEX* Atlas. *(c)–(d)* FUV and NUV aperture magnitudes difference vs aperture magnitudes in *GALEX* Atlas. *(e)* Asymptotic (FUV − NUV) in our catalog vs. that in *GALEX* Altas. *(f)* Aperture (FUV − NUV) in our catalog vs. that in *GALEX* Altas. *(g)–(h)* our C31 and C42 vs. those in *GALEX* Atlas, and the red dashed lines stand for the linear fittings of the galaxies in the NUV.

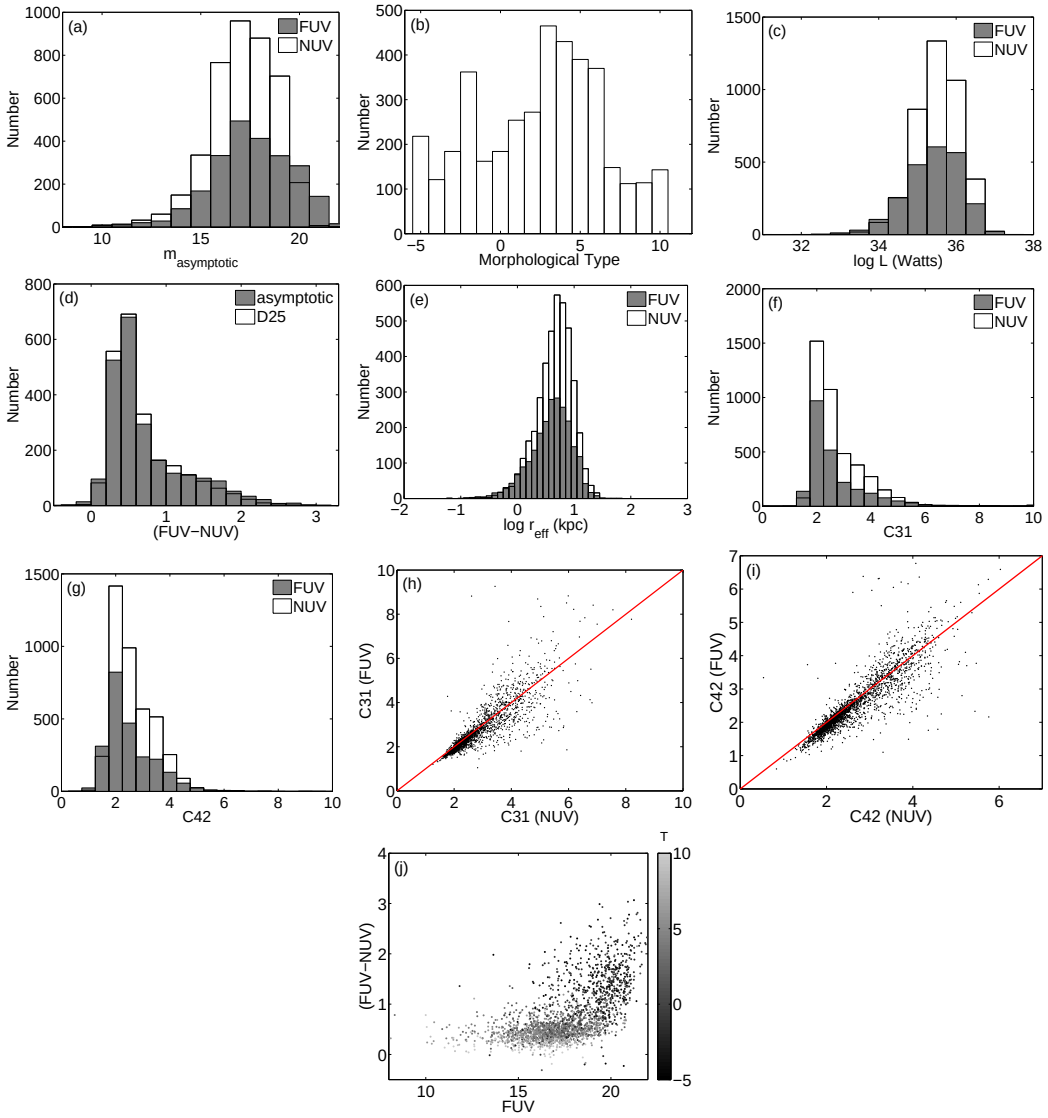

Fig. 5.— Statistical UV properties of our galaxy samples. *(a)* Distribution of asymptotic magnitudes in the FUV (gray-shade) and NUV (solid). *(b)* Distribution of the morphological types. *(c)* Luminosity in watts. *(d)* (FUV-NUV) color. *(e)* Effective radius in kpc. *(f)–(g)* C31 and C42 concentration indices. *(h)–(i)* C31 and C42 in FUV vs. those in NUV. *(j)* Asymptotic (FUV-NUV) color vs. asymptotic FUV magnitudes. The point color reflects the morphology type as shown by the color bar to the right.

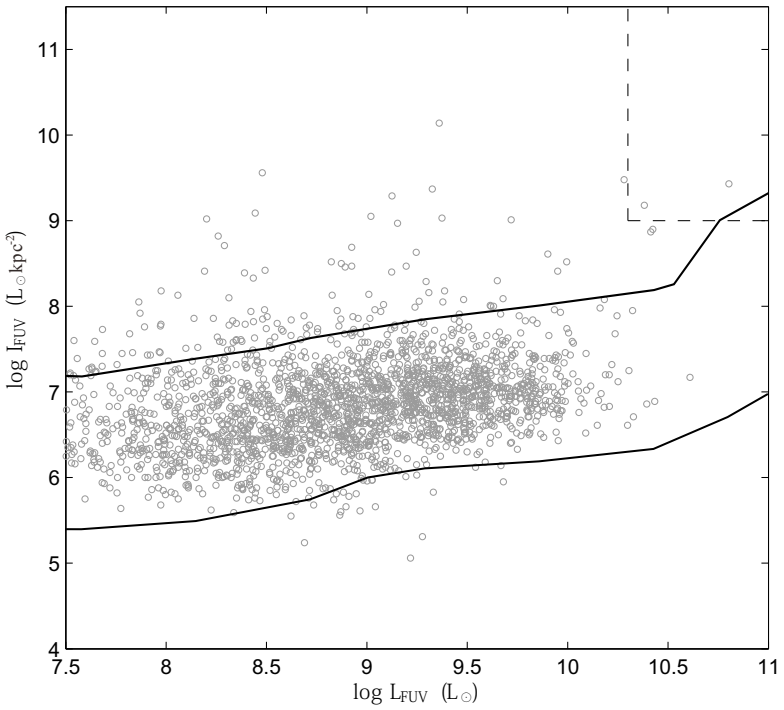

Fig. 6.— FUV surface brightness vs. FUV luminosity. UV properties for the galaxies of our sample are shown as gray empty circles. **The contours stand for the GR1/DR3 sample with FUV detections, which are defined as enclosing 84% of galaxies in the GR1/DR3 sample (Hoopes et al. 2007).** The dashed line shows the region typically populated by LBGs.

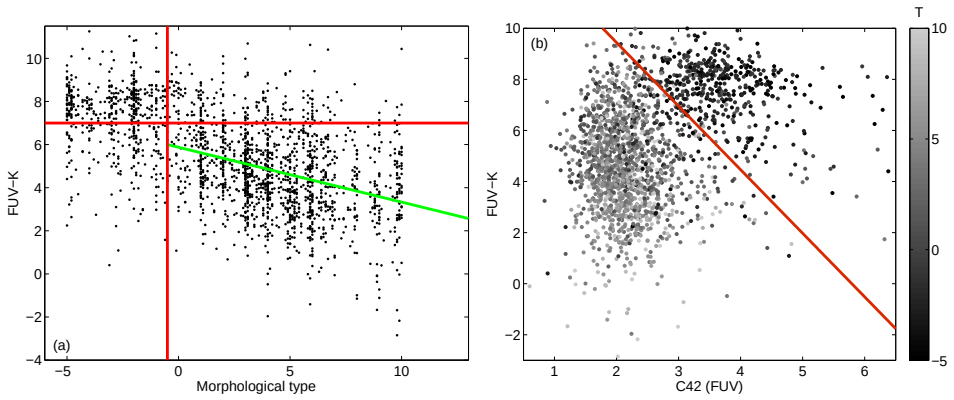

Fig. 7.— *(a)* (FUV - K) vs. galactic morphological type. The red vertical line shows the separation between early and late-type galaxies. The red horizontal line is the demarcation point of (FUV - K) that we use to separate these two types of galaxies. The green line give the linear fit to the relation between (FUV - K) and morphological type for late-type galaxies. *(b)* (FUV−K) vs. the FUV concentration index C42. The point color reflects the morphology type as shown by the color bar to the right, and the red line best separates early and late-type galaxies.

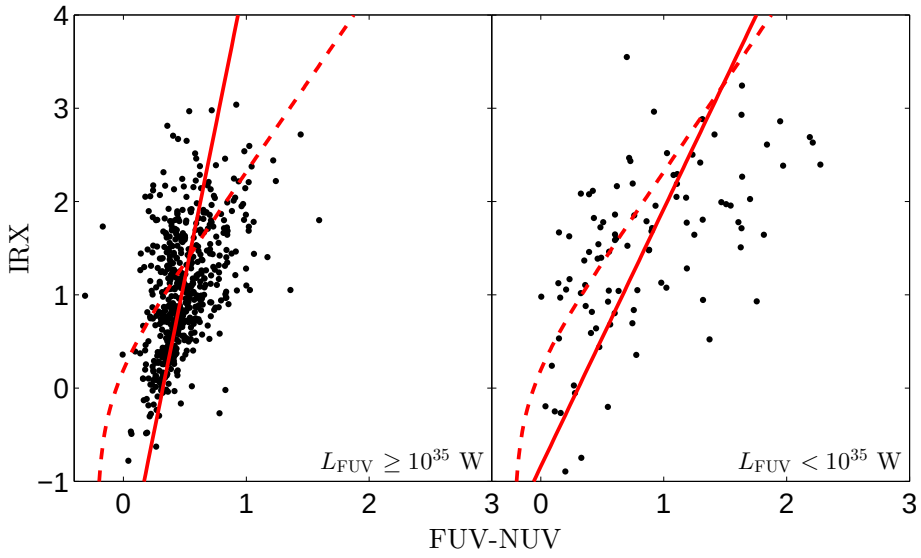

Fig. 8.— IRX-β relations for galaxies with $L_{\rm FUV} \geq 10^{35}$ W (left) and galaxies with $L_{\rm FUV} < 10^{35}$ W (right). The dashed curves show the IRX-β relation of starburst galaxies derived by Meurer et al. (1999). The solid lines are the robust linear fits to the relations of our samples.